**Article:**
Zhang, Longlong, Lu, Xianyang, Wang, Junlin et al. (2021) Shape Defect Effect in Perpendicular Shape Anisotropy Nanodots. IEEE Magnetics Letters. 4501905. ISSN: 1949-307X

https://doi.org/10.1109/LMAG.2021.3088399

# Shape defect effect in perpendicular shape anisotropy nano-dots

Longlong Zhang[1,*], Xianyang Lu[1,*], Junlin Wang[2,1], Lijun Ni[1], Yu Yan[1], Hao Meng[3], Bo Liu[3], Jing Wu[4,1], and Yongbing Xu[2,1]

[1]York-Nanjing International Center of Spintronics (YNICS), Nanjing University, Nanjing 210093, China

[2]Department of Electronic Engineering, University of York, York YO10 5DD, United Kingdom

[3]Key Laboratory of Spintronics Materials, Devices and Systems of Zhejiang Province, Zhejiang Province, P. R. China

[4]Department of Physics, University of York, York YO10 5DD, United Kingdom

**The perpendicular shape anisotropy spin-transfer-torque magnetic random access memory (PSA-STT-MRAM) demonstrates a high thermal stability with the size reduced down to 20 nm, which gives a new way to improve the integrity for electronic devices. This long and narrow device also poses challenges in the device fabrication process, such as sample tilt and etching defect. In this work, we have used a micromagnetic simulation method to investigate the relationship between those defects and device performance. The coercivity and switching current density of the PSA-MRAM have been calculated and analyzed with micromagnetic simulation, 3D Stoner–Wohlfarth model and spin-filter theory. Our results demonstrate how those shape defects affect the performance of the PSA-MRAM and provide guidelines for practical realization of the nano scale PSA-MRAM.**

***Index Terms*—Micromagnetic simulation, MRAM, Spintronics**

## I. Introduction

THE discovery of giant magnetoresistance effect (GMR) has led to tremendous progress in magnetic memory technologies [1, 2]. Magnetization based information devices have remarkable advantages such as non-volatility, high write speed (3–30 ns), high density and low consumption (a few tens of fJ/write). Among these techniques, magnetic random access memory (MRAM) has great potential for further applications, which is based on the magnetic tunnel junction (MTJ). The MRAM device requires the MTJ structure to have a larger tunnel magnetic resistance (TMR) [3, 4]. The magnetization in the ferromagnetic layers in MTJ can be modulated by external field and spin transfer torque [7, 8]. Traditional MRAM cannot be scaled down to 20 nm because of the weak thermal stability [9–12]. Recently, the concept of perpendicular shape anisotropy STT-MRAM (PSA-STT-MRAM) has been proposed [13–15]. In PSA-STT-MRAM, the thickness of the storage layer is drastically increased to values comparable to its diameter. The perpendicular shape anisotropy (PSA) storage layer in the MRAM device can enhance the thermal stability of the device.

Extensive research has shown that material defects in the MTJ structure can influence the performance of MRAM device [16, 17]. For the PSA-MRAM, the shape defect for the storage layer is expected to play an important role in the device. Considering the large thickness and small diameter of the free layer, the fabrication will face serious challenges. The free layer may tilt an angle $\theta$ to it's easy axis as shown in Fig. 1(b) which is different from the ideal shape in Fig. 1(a). Apart from that, during the fabrication process of MRAM, the ion beam etching method may create etching defects in the device. In order to solve the redeposition problem, which is depicted in the Fig. 1(c), the wafers are usually tilted and rotated as shown in Fig. 1(d). The redeposition metallic particles on tunnel barrier are removed by ion beam etching. Due to this special etching method, a new problem might emerge. As shown in Fig. 1(d), the sample might have a cone shape after the ion beam etching process. For the traditional MRAM, the tilt problem and the etching damage may be rather limited as most of the damages are induced in the non-magnetic capping layer. However, as the PSA-MRAM has a very thick free layer of around 20 nm to 80 nm, all these issues related to fabrication process are urgently needed to be resolved.

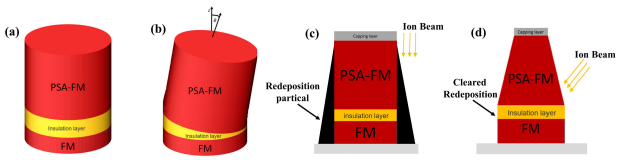


Fig. 1. The defect in PSA-MRAM is induced by etching process. (a) The PSA-MRAM with perfect shape without shape defects. (b) The PSA-MRAM with shape defect which is induce by the easy axis tilt an angle $\theta$ away from the z direction. (c)The redeposition problem induced by vertical etching method. (d) The tilt etching process of MRAM induces a shape defect on the edge of MRAM dots.

In this letter, we report how these fabrication-related structure effects influence the coercivity and switching current density of the free layer in the PSA-MRAM. The micromagnetic simulation and macro spin simulation are used to demonstrate the effects from these defects. It is found that the coercivity and switching current density of the PSA free layer with/without defects can be affected by the tilt angle. The results show that the energy barrier of the PSA free layer can be influenced by the shape defects. The shape defect of the PSA layer will induce a reduction of coercivity and switching current density of the device.

## II. Model and Simulations

The micromagnetic simulations are performed using the Mumax3 simulation package [19], which stands on the

Longlong Zhang and Xianyang Lu contributed equally to this work. Corresponding author: Junlin Wang (Email: junlin.wang@york.ac.uk), Hao Meng (Email: menghao@hikstor.com), Yongbing Xu (Email: ybxu@nju.edu.cn)

Landau-Lifshitz-Gilbert equation. Furthermore, in order to decide the shape parameter of our simulation, a macrospin model is used to calculate the thermal stability factor $\Delta$. The equation is shown as below:

$$\Delta_T = \frac{\pi D^2}{k_B T}[\frac{1}{4}\mu_0 M_s^2 d(1 - \frac{3}{1+4\rho/\sqrt{\pi}}) + K_S + K_u d)] \tag{1}$$

In this work the PSA-dot is assumed to be made of Permalloy. The corresponding parameters are listed as below. Where $k_B$ denote Boltzmann constant $\mu_0$ denotes Permeability, T denotes temperature, and D denotes the diameter of free layer. Also, d is the thickness of the free layer, $\rho = d/D$ is the aspect ratio of the free layer, $M_s = 0.86 \times 10^6$ A/m denotes the saturation magnetization, $K_s = 1.5 \times 10^{-6}$ H/m is the interfacial magnetic anisotropy density and $K_u$ is the magneto-crystalline anisotropy constant, considering the Permalloy is a soft magnetic material and the high interfacial magnetic anisotropy, the $K_u$ is set to 0 to simplify our calculation. The temperature in equation (1) is 300 K. The micromagnetic model is focus on studying the shape defect of the device, which exclude the thermal effect.

Fig. 3(a) is the phase diagram of the result, calculated by equation (1). With a relative small diameter of 10 nm, both the ferromagnetic layers with the thicknesses of 25 nm and 60 nm achieve a strong perpendicular shape anisotropy ($\Delta$ around 70 and 280). In the discussion below, these two sets of ferromagnetic layer parameters(until otherwise specified) are utilized.

The precessional processes of magnetic moments is commonly explained by the Landau-Lifshitz-Gilbert-Slonczewski (LLGS) equation which given as below[19]:

$$\frac{d\vec{m}}{dt} = -\frac{\gamma H_{eff}}{1+\alpha^2}\vec{m_p}\times\vec{m} + \frac{\alpha\gamma H_{eff}}{1+\alpha^2}\vec{m_p}\times(\vec{m_p}\times\vec{m}) - \frac{J^Q\hbar}{M_s e d}\frac{\epsilon-\alpha\epsilon^*}{1+\alpha^2})\vec{m_p}\times(\vec{m_p}\times\vec{m}) + \frac{J^Q\hbar}{M_s e d}\frac{\epsilon-\alpha\epsilon^*}{1+\alpha^2})\vec{m_p}\times\vec{m} \tag{2}$$

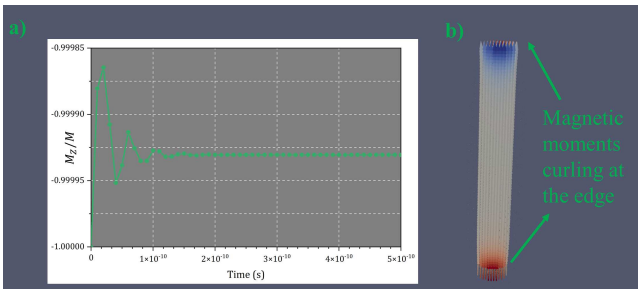


Fig. 2. (a) the magnetic moments variation in the relaxation process. (b) the free layer shows curling magnetic moments at the edge.

In this equation $\gamma$, $H_{eff}$, e, $\hbar$ and $\alpha$ denotes the gyromagnetic ratio, effective field, electron charge, reduced Planck Constant and Gilbert damping constant respectively, $\vec{m}$ is the unit vector of the free layer magnetic moment, $\vec{m_p}$ is the unit vector of the pined layer magnetic moment, $J^Q$ is the current density. $\epsilon$ and $\epsilon^*$ are the spin-torque parameters. Obvious,when the magnetization direction of the free layer and pinned layer are parallel(the tilt angle $\theta = 0$), the LLGS equation(2) equals to zero. Exclude the thermal fluctuation, there lack a initial angle $\theta$ to trigger the precessional processes. In the PSA-MRAM, there is something different to the traditional MRAM model, the demag filed will curling the edge magnetic order of the magnetic free layer and triggered the precessional processes, as shown in the Fig. 2(a) . In the PSA-MRAM the perpendicular shape anisotropy in other words the demag filed play a dominant role in the magnetization switching process.

## III. Results and Discussion

### A. The relationship between tilt angle ($\theta$) and the performance of MRAM device

The relationship between tilt angle ($\theta$) and the performance of MRAM device is carefully studied in the first place. For the coherent switching mode, angular dependence of coercivity is given by equation(2) [6, 21].

$$H_n^c(\theta) = -\frac{2[K_{sh}(L_{nw}) + K_u]\sqrt{1-\beta^2+\beta^4}}{\mu_0 M_s^2(1+\beta^2)} M_s \tag{3}$$

where $\beta = tan(\theta)^{1/3}$, and $\theta$ is the angle between the applied field and long axis of the free layer; $L_{nw}$ represents the length of the nanowire, and $K_{sh}(L_{nw})$ denotes the shape anisotropy constant.

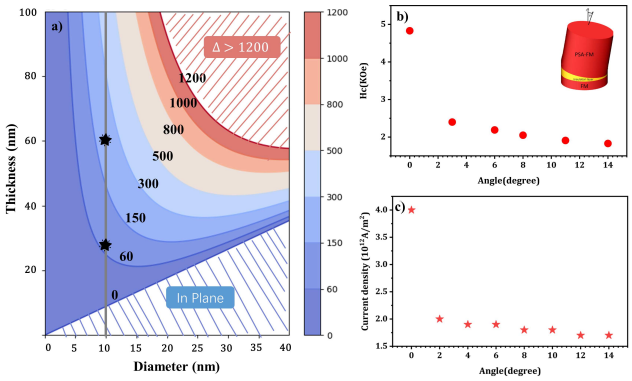


Fig. 3. (a)Thermal stability phase diagram of MTJ device versus the thickness of free layer d and diameter D, at room temperature (300K). The tilt angle dependent (b) coercivity and (c) switching current density of PSA nano dot. The tilt angle $\theta$ is changed from 0 degree to 14 degrees, The diameter and the thickness of the nano dot are set as 10 nm and 25 nm respectively.

From the simulation results shown in Fig. 3(b), the coercivity of the free layer is found to be dependent on the tilt angle $\theta$. When $\theta$ = 0, the free layer has a large coercivity around 5000 Oe, which is comparable with previous reports [21, 22]. This relatively high coercivity might be attributed to the large energy barrier ($E_B = \Delta \times k_B T$) induced by perpendicular shape anisotropy. With $\theta$ increased from 0 to 10 degree, the coercivity sharply drops to a value around 2000 Oe. The simulation results show that the magnetization of the PSA-MRAM is relatively hard to switch by the external field. On the other hand, the results demonstrate that the tilt angle has a strong effect on the coercivity of PSA-MRAM.

The relationship between the tilt angle $\theta$ and switching current density $J_c$ has also been studied. The small tilt angle $\theta$ in the MRAM free layer will also bring a significant impact on the switching current density. Deduced from the equation(3) we can the the analytical solution between the tilt angle($\theta$) and switching current density $J_c$:

$$J_c(\tau) \propto J_{c0}[1 + \frac{(ln\frac{\pi}{2\theta_{Tilt}})}{(\frac{\tau}{\tau_0})}] \quad (4)$$

In this equation $J_{c0}$ is the intrinsic current density required for current driven magnetization reversal in a MTJ. $\tau_0 \sim 1ns$ is the inverse of the attempt frequency, and $\tau$ is the current pulse width. Then, the diameter and the thickness of the nano dot are assumed to be 10 nm and 25 nm, respectively. The current pulse duration is fixed at 3 ns. The switching current density is shown in Fig. 3(c). With $\theta$ = 0, the switching current density is $4.0 \times 10^{12}$ A/m$^2$, which is obvious larger than the tradition MRAM device [15]. The relatively large switching current density is also origin from the high energy barrier between PSA-MRAM's two magnetic state. However, with a small tilt angle $\theta$, the switching current density drops half to $2.0 \times 10^{12}$ A/m$^2$, similar to the previous research results [15]. The results show that the larger tilt angle of the system, will reduces the switching current density. The micromagnetic simulation results is in good agreement with the analytical solution (calculated by the equation 4) which is given in Fig. 3.

Besides, the tilt angle $\theta$ will increase the speed of magnetic switching in PSA layer. As shown in the Fig. 4(a), when tilt angle equal to 0 degree, the magnetization switching in PSA layer is completed at around 3.0 ns. As shown in the Fig. 4(b), when the tilt angle increased to 4 degree, the time for the magnetization switching in PSA layer is around 1.5 ns. As shown in the Fig. 4(c), when increase the tilt angle once more to 12 degree, the time for the magnetization switching will drop to around 1.3 ns.

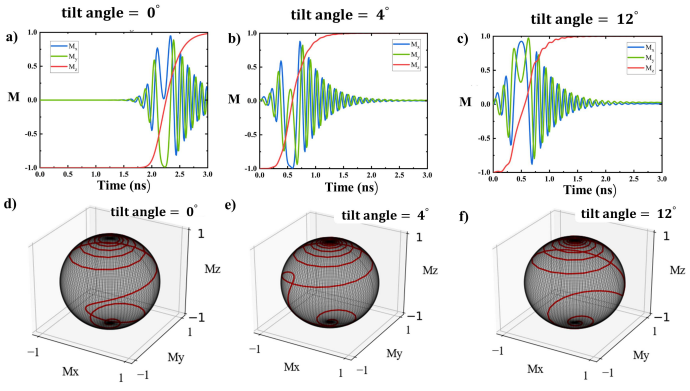


Fig. 4. Magnetization profile under spin-torque effect for four different tilt angles. The pulse width and current density were fixed to 3 ns and $4.0 \times 10^{12} A/m^2$, respectively. The free layer thickness is 25 nm.

Indicate to illustrate this phenomenon more clearly, we adapt a sequence of increasing current density and show the Time to Magnetization figures. The results in Fig. 5 all approve the conclusion that the tilt angle $\theta$ accelerates the switching switching in PSA layer.

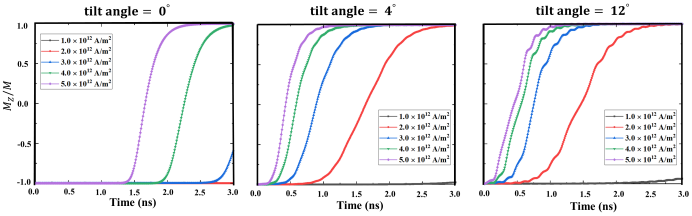


Fig. 5. A sequence of magnetization profile under spin-torque effect for four different tilt angles. The free layer thickness is 25 nm.

### *B. The relationship between etching defects and the performance of MRAM device*

The exchange length in the sample with large thickness, is shorter than the physical thickness, which is insufficient for supporting a coherent switching mode. For samples with small thickness, the magnetization switching approximately coherent. As shown in Fig. 6(a), for the thicker sample, the free layer can be seen as a nanowire and there will have magnetic domain wall nucleation at the edge of the free layer [23, 24]. As shown Fig. 6(b), for the thicker sample, the whole switching process can be divided in to two steps: domain nucleation and domain wall propagation.

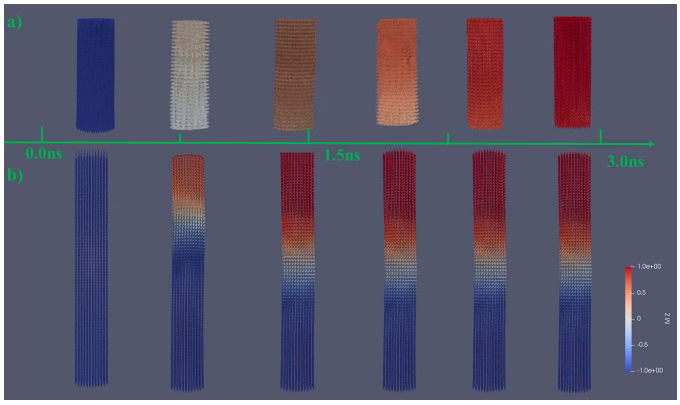


Fig. 6. Two different switching modes for magnetic free layer with different thicknesses. (a) the 25 nm thickness sample is switched by current in a coherent mode (b) the 60 nm thickness sample is switched by current in a transverse wall mode.

The effect of the etching defect in PSA-MRAM with different thicknesses has been studied by the micromagnetic and Stoner-Wohlfarth model simultaneously. Here we define defect "level" as a parameter to describe the ratio between the top area and bottom area of the free layer. The detailed shape defect levels of the nano dot are defined as Level 0 to 3, which are exhibited in the insets Fig. 7(a). Level 0 is a defect free case, and the Level 1-3 represent different extents of etching defect.

The relationship between the device coercivity and etching defects is given in Fig. 7. Two groups of samples with different thicknesses (25 nm and 60 nm) are simulated. The diameters are fixed at 10 nm. Besides, various tilt angles of applied field are considered in the calculation. The results show that the device coercivity is decreased with the etching defect. As shown in Fig. 7(a), the simulation of defect-free nano dot

(Level 0) with a thickness of 25 nm is in good agreement with the Stoner-Wohlfarth model of the coherent mode [21]. For the etching defect samples with Level 1 to Level 3, the geometric symmetry of the nano dot is broken which reduce the coercivity. As shown in Fig. 7(b), for the structures with 60 nm, the coercivity trend deviates from the value calculated by the coherent switching mode for the defect-free case (Level 0). This is due to the fact that the transverse wall switching mode lowers down the energy barrier between the parallel magnetic state to anti-parallel state.

The relationship between switching current density and etching defect level is studied by micromagnetic method and macrospin model at the remainder of this article. For the nano dots with thickness of 25 nm as shown in Fig. 7(c), the etching defect demonstrates a significance influence on the switching current density. For the defect-free samples (Level 0), the simulation result is consistent with the analytical solution [25–27]. However, for the structures with etching defects(Level 1-3 samples) the switching current density is smaller than defect-free nano dot (Level 0), which indicating a significant impact on the device demagnetization field and energy barrier caused by the etching defect in the nano dot shown in the Fig. 7(e).

For the 60 nm nano dot, the switching process is dominated by the domain wall motion. Thus the defect-free samples (Level 0) show a huge deviation from the analytical solution which is deduced by the coherent switching mode in Fig. 7(d). The etching defect in the 60 nm dot does not bring significant effect to switching current density. This is probably due to the magnetic switching process in the 60 nm dots is totally different from the 25 nm samples. The current induce domain nucleation at the interface of the free layer is shown in Fig. 6(b). The etching defect at interface is much smaller than the defect in free layer. The gradient shape defects of the free layer gives a weak influence on the domain nucleation process. As shown in Fig. 7(d), the etching defect does not have an obvious effect to the nucleation current density. It is necessary to point out that the 60 nm structure cannot be switched completely by a pure interface STT effect. This is due to the fact that the Permalloy has a relative short exchange length ($L_{ex}$ = 5.35 nm), and thus the interface STT effect cannot take a dominant role in the long range magnetic order. The motion of domain wall is induced by the Zhang-Li torque, which drive the domain motion in the nanodot until saturation.

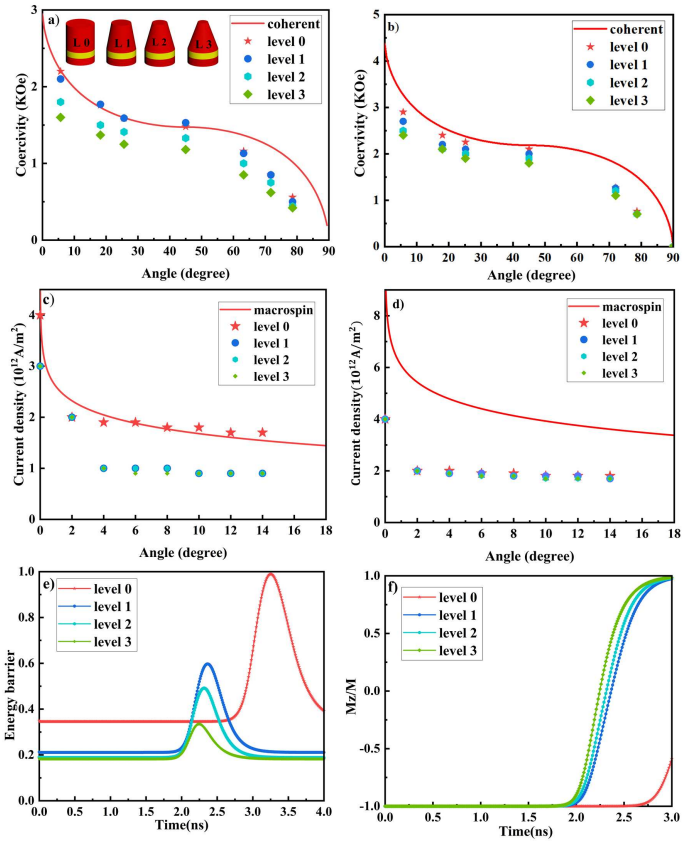


Fig. 7. Angular dependence of coercivity for (a) 25 nm and (b) 60 nm nano dots. The red solid line is the analytical solution of coherent switching mode which is calculated by 3D Stoner–Wohlfarth model. (c) Angular dependence of switching current density for 25 nm nano dots. (d) Angular dependence of nucleation current density for 60 nm nano dots. The red solid line is the analytical solution of coherent switching mode deduced by equations 3. (e) The total energy evolution map in the magnetic moment switching process. (f) Simulation result of the switching time with respect to the level of etching defect for 25 nm sample. The lower extent of the etching defect the faster the switching process.

## IV. Conclusion

In conclusion, we have found that IBE fabrication process induced the etching defect and pillar tilt and patterning process strongly influence the performance of the PSA-MRAM. The micromagnetic simulation, 3D Stoner–Wohlfarth model and spin-filter theory show that the tilt angle reduces the coercivity of the free layer which affects the stability of the information storage in PSA-MRAM. We have further demonstrated that the magnetization switching mode in free layer depends on its thickness. The different switching modes influence the performance of PSA-MRAM device such as the magnetic domain wall nucleation and the shape anisotropy gradient. Our results provide useful insight into the designing and development of the PSA-MRAM devices.

The data that support the findings of this study are available from the corresponding authors upon reasonable request.

## Acknowledgment

This work is supported by National Key Research and Development Program of China (Grant No. 2016YFA0300803), the National Natural Science Foundation of China (Grant No. 61427812, 11774160), the Natural Science Foundation of Jiangsu. Province of China (No. BK20192006), the Fundamental Research Funds for the Central Universities (Grant No. 021014380113) the Natural Science Foundation of Jiangsu Province of China (No. BK20200307.

## REFERENCES


[1] M. N. Baibich, J. M. Broto, A. Fert, F. N. Van Dau, F. Petroff, P. Etienne, G. Creuzet, A. Friederich, and J. Chazelas, Phys. Rev. Lett. **61**, 2472 (1988).

[2] G. Binasch, P. Grünberg, F. Saurenbach, and W. Zinn, Phys. Rev. B **39**, 4828 (1989).

[3] S. Tehrani, B. Engel, J. Slaughter, E. Chen, M. DeHerrera, M. Durlam, P. Naji, R. Whig, J. Janesky, and J. Calder, IEEE Trans. Magn. **36**, 2752 (2000).

[4] N. Nishimura, T. Hirai, A. Koganei, T. Ikeda, K. Okano, Y. Sekiguchi, and Y. Osada, J. Appl. Phys. **91**, 5246 (2002).

[5] N. Liebing, S. Serrano-Guisan, K. Rott, G. Reiss, J. Langer, B. Ocker, and H. Schumacher, Phys. Rev. Lett. **107**, 177201 (2011).

[6] J.-G. J. Zhu and C. Park, Materials today **9**, 36 (2006).

[7] L. Thomas, G. Jan, J. Zhu, H. Liu, Y.-J. Lee, S. Le, R.-Y. Tong, K. Pi, Y.-J. Wang, D. Shen, et al., J. Appl. Phys. **115**, 172615 (2014).

[8] Y. Shiota, T. Nozaki, S. Tamaru, K. Yakushiji, H. Kubota, A. Fukushima, S. Yuasa, and Y. Suzuki, Appl. Phys. Express **9**, 013001 (2015).

[9] K. Tsunekawa, D. D. Djayaprawira, M. Nagai, H. Maehara, S. Yamagata, N. Watanabe, S. Yuasa, Y. Suzuki, and K. Ando, Appl. Phys. Lett. **87**, 072503 (2005).

[10] W. Zhao, X. Zhao, B. Zhang, K. Cao, L. Wang, W. Kang, Q. Shi, M. Wang, Y. Zhang, Y. Wang, et al., Materials **9**, 41 (2016).

[11] J. J. Kan, C. Park, C. Ching, J. Ahn, Y. Xie, M. Pakala, and S. H. Kang, IEEE T ELECTRON DEV **64**, 3639 (2017).

[12] T. Endoh, S. Kang, T. Kudo, and Y. Yagi, in 2018 IEEE International Magnetics Conference pp. 1–1 (2018).

[13] N. Perrissin, S. Lequeux, N. Strelkov, A. Chavent, L. Vila, L. D. Buda-Prejbeanu, S. Auffret, R. C. Sousa, I. L. Prejbeanu, and B. Dieny, Nanoscale **10**, 12187 (2018).

[14] N. Perrissin, G. Gregoire, S. Lequeux, L. Tillie, N. Strelkov, S. Auffret, L. Buda-Prejbeanu, R. Sousa, L. Vila, B. Dieny, et al., J. Phys. D: Appl. Phys. **52**, 234001 (2019).

[15] K. Watanabe, B. Jinnai, S. Fukami, H. Sato, and H. Ohno, Nat. Commun. **9**, 1 (2018).

[16] A. Chintaluri, A. Parihar, S. Natarajan, H. Naeimi, and A. Raychowdhury, A model in 2015 IEEE 24th Asian Test Symposium (ATS) pp. 187–192 (2015).

[17] L. Wu, M. Taouil, S. Rao, E. J. Marinissen, and S. Hamdioui, in 2018 IEEE International Test Conference (ITC) pp. 1–10 (2018).

[18] A. Chintaluri, H. Naeimi, S. Natarajan, and A. Raychowdhury, IEEE Journal on Emerging and Selected Topics in Circuits and Systems **6**, 319 (2016).

[19] A. Vansteenkiste, J. Leliaert, M. Dvornik, M. Helsen, F. Garcia-Sanchez, and B. Van Waeyenberge, AIP Adv. **4**, 107133 (2014)

[20] J. Wang, X. Zhang, X. Lu, J. Zhang, Y. Yan, H. Ling, J. Wu, Y. Zhou, and Y. Xu, Appl. Phys. Lett. **111**, 072401 (2017).

[21] L. Vivas, M. Vazquez, J. Escrig, S. Allende, D. Altbir, D. Leitao, and J. Araujo, Phys. Rev. B **85**, 035439 (2012).

[22] H. Li, M. Yue, Y. Peng, Y. Li, Q. Wu, W. Liu, and D. Zhang, in 2017 IEEE International Magnetics Conference (INTERMAG), 1 (2017).

[23] R. Hertel and J. Kirschner, Physica B: Condensed Matter, **343**, 206 (2004).

[24] J. Cai, B. Fang, C. Wang, and Z. Zeng, Appl. Phys. Lett. **111**, 18 (2017).

[25] Y. Huai et al., AAPPS bulletin **18**, 33.

[26] C.-M. Lee, J.-S. Yang, and T.-h. Wu, IEEE T. Magn. **47**, 649 (2011).

[27] N. N. Mojumder and K. Roy, IEEE. T. Electron. Dev. **59**, 3054 (2012).